Auto-oscillation thresholds at the main resonance in ferrimagnetic films

A. Prabhakar*
Department of Physics, Carnegie Mellon University, Pittsburgh, Pennsylvania 15213

D. D. Stancil
Department of Electrical and Computer Engineering, Carnegie Mellon University, Pittsburgh, Pennsylvania 15213
(Received 25 August 1997)

The propagation of large-amplitude forward-volume magnetostatic waves (MSW's) is studied in $Y_3Fe_5O_{12}$ and $[BiLu]_3Fe_5O_{12}$ thin films. The onset of auto-oscillations beyond the second Suhl instability influences the transmission characteristics of a MSW delay line. Global variations in transmitted power over a frequency-power input parameter space are monitored using density plots. There is a shift in the MSW passband with increasing input power that is explained by a decrease in demagnetizing field with an increase in dynamic magnetization. As the input power increases beyond a threshold value, we observe an increase in signal amplitude, heralding the onset of auto-oscillations. Fingers of auto-oscillation spanning an input range of 200 MHz and 10 dB are formed. The locations of these fingers are correlated with the locations of spin-wave resonance notches in the MSW passband. The auto-oscillation thresholds in the vicinity of a spin-wave resonance notch are 4–8 dB lower than elsewhere in the passband. A heuristic model based on a reduced group velocity near a notch can explain the lower threshold values. [S0163-1829(98)02018-9]

I. INTRODUCTION

The study of parametrically excited spin waves has become the subject of active research over the last few years.[1–4] Ferrimagnetic materials, particularly garnets, have been extensively used to probe the dynamic properties of the spin-wave manifold. The spin-wave system allows us to calculate Lyapunov exponents and fractal dimensions and to observe multiple routes to chaos.[5,6] Hopf bifurcations,[7] period doubling,[8] formation and destruction of overlapping attractor basins,[9] intermittency,[10] mode locking, and synchronization of chaos[11,12] are some of the demonstrated behavioral patterns in a spin-wave system.

A forward-volume magnetostatic wave (MSW) delay line is a commonly used experimental device. The normalized transmission characteristics (S_{12}) of the delay line are usually described as a passband in the frequency domain measured at low values of input power. However, the high-power characteristics are significantly different. This article illustrates the use of a density or contour plot of S_{12} as an investigative tool. Such a plot gives a researcher the ability to pinpoint regions where chaotic phenomena are most prevalent in a two-dimensional input parameter space consisting of frequency and power. Considering the vastness of the parameter space, approximately 400 MHz$\times$20 dB, this in itself proves valuable. At high-power levels, we witness the collective oscillation of the spin-wave system at a frequency of 10^4–10^6 Hz. This phenomenon is commonly referred to as auto-oscillations. Interestingly enough, a density plot also allows us to draw general conclusions about the onset and the formation of fingers of auto-oscillation. This phenomenon was previously studied in a nondegenerate spin-wave manifold on circular films.[13,14] We investigate the case of propagating forward-volume MSW's, where the degeneracy between thickness modes is lifted with the inclusion of a spin-wave exchange interaction energy.[15,16] The inclusion of an exchange term leads to the formation of spin-wave resonance notches or dipole gaps. For spin waves pinned to the surface of the film, the spacing between dipole gaps determines the mode numbers associated with the interacting spin waves.[17] The lowest-order thickness mode is the predominantly excited mode and a dipole gap is a characteristic of an interaction between the lowest mode and a higher-order mode. Using a density plot, we correlate the existence of dipole gaps with the formation of fingers of auto-oscillation.

The group velocity for spin waves within a dipole gap is smaller than that of the lowest-order mode.[18] A lower group velocity also implies a longer propagation time between transducers and thus less transmitted power. The dipole gaps break up a density plot of S_{12} into alternating peaks and valleys. With the inclusion of higher-order demagnetizing effects in the MSW dispersion relation, the location of the MSW passband becomes dependent on the spin-wave amplitudes. An increase in input microwave power causes a shift in the passband to a higher frequency. A density plot easily captures this phenomenon, and the valleys formed by the dipole gaps appear shifted towards higher frequencies at higher-power levels.

Density plots of S_{12} using MSW delay line also reveal the peculiar formation of fingers of low transmission.[19] This phenomenon shall be explored in greater detail using three ferrimagnetic thin film samples having different material and geometrical properties. The threshold input power associated with the formation of these fingers approximately coincides with a predicted value for the auto-oscillation threshold in an infinite medium. The standard procedure of exciting spin waves using well-characterized resonators is not employed. While resonators are easier to characterize, delay lines using propagating modes in thin films are also of great practical interest. Due caution is necessary when comparing experimental observations on a thin film delay line with theoretical predictions for spin waves in an infinite medium. Sample

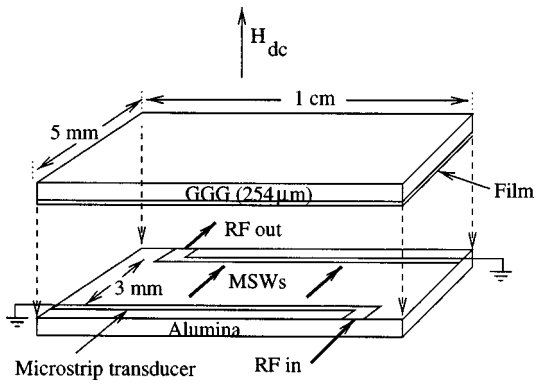

FIG. 1. Schematic of a MSW delay line. Typical dimensions for the device are shown, although some experiments were run using films with arbitrary shapes and with a wider separation between transducers. The transducers are 50 μm wide, and the film is pressed into physical contact with them.

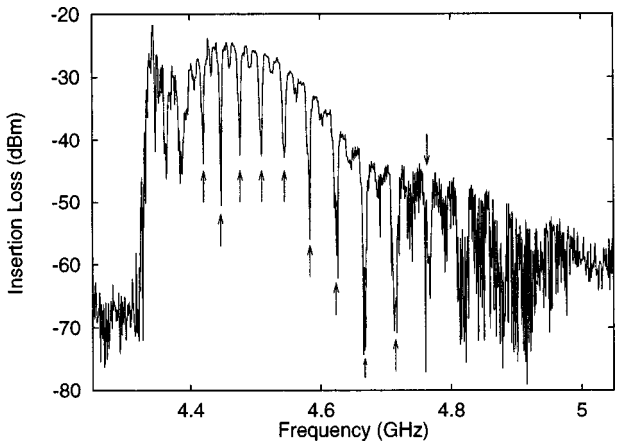

FIG. 2. MSW passband for sample YIG1 in the presence of a 270 kA/m (3.40 kOe) external magnetic field. The passband was measured using a network analyzer while sweeping the input frequency in steps of 1 MHz. The arrows mark the approximate locations of notches identified as dipole gaps.

calculations that facilitate such a comparison are presented with a clear demarkation of the various approximations at each step.

A finger of auto-oscillation can be interpreted as a small range of input frequencies over which the threshold power required to observe auto-oscillations is lower than elsewhere in the passband. Assuming a uniform coupling of power into spin-wave modes at all frequencies, a lower group velocity for a wave causes the magnetic energy density in the film to be larger within a dipole gap. Consequently, we expect a lower auto-oscillation threshold in the vicinity of a gap. The existence of multiple regions of lower group velocity combined with a shift in the passband leads to the formation of fingers of auto-oscillation. The decrease in threshold power values for observing auto-oscillations is estimated based on a heuristic model of a higher energy density inside a dipole gap. The estimates compare favorably with our experimental observations.

II. EXPERIMENTAL RESULTS

A schematic of the experimental device is shown in Fig. 1. The properties and physical dimensions of the yttrium-iron garnet (YIG) and bismuth-lutetium-iron garnet (BLIG) films that were used in our experiments are listed in Table I. An external field H_{dc} was applied perpendicular to the plane of the film and forward-volume MSW's were excited by a microstrip transducer in contact with the film surface. A second transducer acted as a receiver. A large separation between transducers, of 1 cm, was initially used to minimize the effects of stray electromagnetic fields on the transmission characteristics. However, the larger propagation length for the MSW's caused a strong attenuation of the signal. Since nonlinear excitations decay rapidly with propagation distance, the separation between transducers was reduced to either 3 or 4 mm for a high-power experiment. The use of rectangular films whose width was comparable to the spacing between transducers raises the possibility of multipath interference. This issue shall be addressed in Sec. II B. Low-power experiments were conducted using a network analyzer. However, the instrument had a large insertion loss of approximately 17 dB. Hence, for high-power experiments, the network analyzer was replaced by a diode detector whose output was fed to a digital oscilloscope. Results from both the low- and high-power experiments are presented below.

TABLE I. Physical dimensions and ferromagnetic resonance (FMR) linewidth of the films used. The rectangular films had polished edges.

Film	Shape	Dimensions	ΔH_{FMR} (at 9.1 GHz)
YIG1	Quadrant	1.0 in (radius)$\times$5.9 μm	0.6 Oe
YIG2	Rectangle	$10\times5\mathrm{mm}^2\times7.4$ μm	0.87 Oe
BLIG	Rectangle	$15\times5\mathrm{mm}^2\times6.3$ μm	3.0 Oe

A. MSW passband

Figure 2 is a typical low-power forward-volume MSW passband, using transducers that were 1 cm apart and external field $H_{\mathrm{dc}}=270$ kA/m. The rapid oscillations at the low and high ends of the passband are an indication of stray electromagnetic fields. The irregular shape of the sample, its rough edges, and the large separation between transducers reduced the effects of multipath interference and stray electromagnetic coupling between the transducers. The edge of the passband was determined by the strength of the internal magnetic field. We use the data in Fig. 2 to estimate the anisotropy field H_k while assuming a typical value for the saturation magnetization, $M_s=140$ kA/m. Identifying the edge of the passband as $\omega_H=2\pi$ (4.35 GHz), we find the anisotropy field to be

$$H_k\approx\frac{\omega_H}{|\gamma|\mu_0}-H_{\mathrm{dc}}+M_s=-6.4\ \ \mathrm{kA/m}, \tag{1}$$

where $\gamma=-2\pi(28\ \mathrm{GHz/T})$ is the gyromagnetic ratio and μ_0 is the permeability of free space. Thus anisotropic effects account for less than 5% of a change in the internal magnetic field.

The presence of notches in Fig. 2, marked by the arrows, indicates a coupling to exchange-dominated spin-wave

resonances.[17] A smooth passband, without any notches, is a characteristic of a lowest-order excitation. Neglecting anisotropy while retaining exchange and dipolar interactions gives the dispersion relation[20]

$$\omega^2=(\omega_H+\omega_M\lambda_{ex}k^2)[\omega_H+\omega_M(\lambda_{ex}k^2+\sin^2\theta)], \quad (2)$$

where k is the MSW wave number, $\omega_M=-\gamma\mu_0 M_s$, and θ is the propagation angle with respect to H_{dc}. The value of the exchange constant λ_{ex} can be determined from microwave frequency measurements.[21] Experimentally, it was observed that the spin waves behaved as if they were pinned to the surfaces of the film. Reflections at the top and bottom surfaces caused a spin-wave resonance notch when the film thickness equaled an integral number of half wavelengths. Assuming $\theta\rightarrow 0$, since the tangential wave number $k_t \ll k$, the resonant frequencies are obtained from Eq. (2) as

$$\omega_n=\omega_H+\omega_M\lambda_{ex}\left(\frac{\pi n}{d}\right)^2, \quad n=1,2,3,\ldots . \quad (3)$$

The subscript n is chosen to represent the number of zeros in the magnetostatic potential for a mode through the thickness of the film. The mode number associated with each gap is determined by assuming uniform pinning of spin waves on both surfaces of the film and then measuring the increase in frequency separation between gaps as n increases. The relative coupling strength of the external magnetic field to the even and odd modes must be accounted for to ensure proper mode enumeration. The external field varies slowly on the scale of the film thickness, and the strongest excited mode is the $n=0$ mode whose magnetostatic potential is described by

$$\psi(\vec{r})=\psi_0 e^{-j\vec{k}_t\cdot\vec{r}}\cos\left(\frac{\pi z}{d}\right), \quad -d/2>z>d/2, \quad (4)$$

$$\psi_0=\sqrt{\frac{2P}{\omega\mu_0}}, \quad (5)$$

where P is the power per unit width coupled into the wave. This mode is usually orthogonal to modes with higher-order thickness variations. However, in the presence of surface pinning, coupling to other modes can occur when the frequencies are degenerate. The coupling is stronger for modes having the same even symmetry in ψ. Hence it is reasonable to conclude that the notches in Fig. 2 correspond to even mode numbers. Evidence of a weaker coupling to odd-numbered spin-wave resonant modes can be seen between the deep notches in Fig. 2. The spin-wave spectrum with mixed exchange boundary conditions was studied by Kalinikos and Slavin using perturbation theory.[18] Some of their results are utilized in Sec. III to estimate the MSW group velocity in the vicinity of a dipole gap.

Having established that the dipole gaps seen in Fig. 2 are primarily due to a spin-wave resonance phenomenon associated with even modes, Eq. (3) is rewritten as

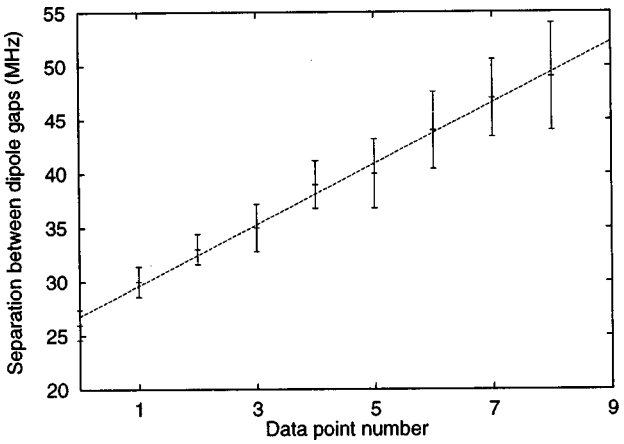

FIG. 3. Increasing frequency separation between the dipole gaps seen in Fig. 2. The solid line is a least squares fit given by $\Delta f(\mathrm{MHz})=2.83m+26.8$ with $\chi^2=3.2$. The mode number that identifies a gap is merely $2m+n_0$ where $n_0=2(26.8/2.83)-1\approx 18$.

$$\Delta f=\frac{1}{2\pi}(\omega_{n+2}-\omega_n)$$

$$=\frac{2\pi\omega_M\lambda_{ex}}{d^2}(n+1), \quad n=0,2,4,\ldots . \quad (6)$$

Thus a plot of Δf versus n should be linear with a definite relation between the slope and the intercept. Likewise, Δf versus $(n-n_0)$ is linear, where n_0 is the mode number of the first observable gap. If this data fits a line having the form $y=am+b$, $m=0,1,2,\ldots$, then the mode number associated with the first gap is uniquely determined by making the identifications

$$2m=n-n_0, \quad (7)$$

$$n_0=\frac{b}{a}-1, \quad (8)$$

with n_0 being defined as an even integer. Given the thickness of the film and the saturation magnetization, it is also possible to determine the exchange constant as

$$\lambda_{ex}=\frac{a}{2}\left(\frac{d^2}{2\pi\omega_M}\right). \quad (9)$$

Figure 3 is a plot of Δf versus m. Using a least squares fit, we determined that the dipole gap at 4.421 GHz has a mode number $n_0=18$. With $d=5.9$ μm and $M_s=140$ kA/m, $\lambda_{ex}=2.5\times 10^{-16}$ m^2. This value is in good agreement with a typical value of $\lambda_{ex}\sim 3\times 10^{-16}$ m^2 for YIG.[21]

On a practical note, the spin-wave resonance absorption lines are undesirable for many device applications. However, their presence can be minimized by properly orienting the film in the external magnetic field.[22,23]

B. Fingers of auto-oscillation

Figure 4 shows a density plot of S_{12} using transducers that were 4 mm apart and the sample, YIG1, whose passband was shown in Fig. 2. The dipole gaps appear as dark bands that

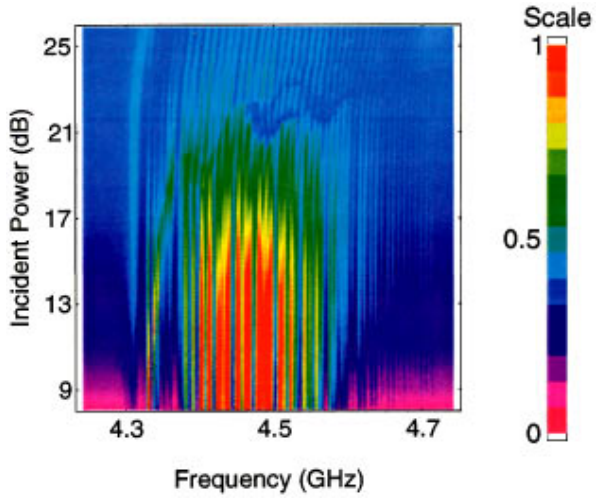

FIG. 4. (Color) Density plot of S_{12} over input parameter space using sample YIG1.

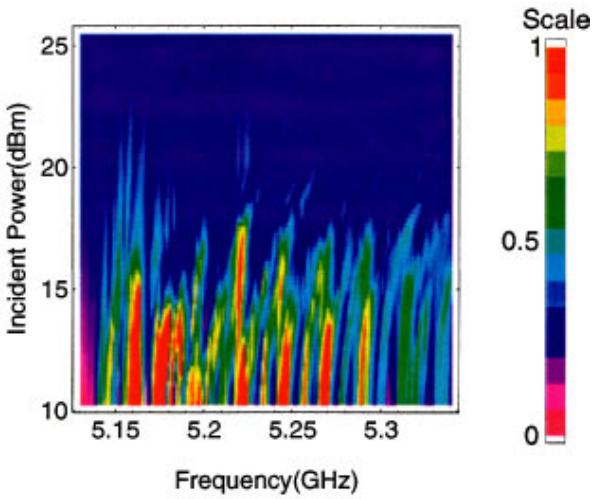

FIG. 6. (Color) Density plot of S_{12} for sample YIG2. Note the formation of fingerlike regions of low transmission (dark regions extending down from above) around 15 dBm.

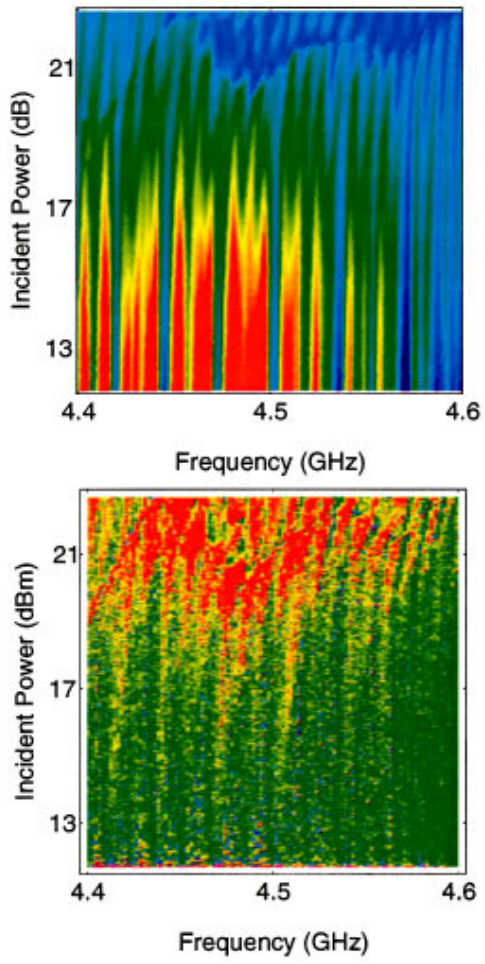

FIG. 5. (Color) Top: magnified view of S_{12} from Fig. 4, with red regions corresponding to strong transmission. Bottom: density plot of peak-to-peak voltage from a time series measurement at a fixed input power and input frequency, with red regions corresponding to strong nonlinear excitations.

show the characteristic increasing separation with higher mode numbers. Measurements of the reflected power indicated that the waviness in the pattern visible at high power is related to the length of the connecting coaxial cables. The appearance of the pattern helps us make a comparison between different density plots, and it shall be used to our advantage.

We now select a small region of our input parameter space. At the top of Fig. 5 is a magnified view of the density plot over the selected region. Interestingly enough, the spin-wave resonances corresponding to odd mode numbers, which were suppressed at low-input-power levels, were also strongly excited. The dipole gaps corresponding to the odd modes, visible as small dips between the even gaps in Fig. 2, became as strong as their even counterparts and caused the passband to break up into alternate regions of strong and weak transmission. In the density plot, at $\sim$12 dBm, the odd dipole gaps appear as faint streaks between the darker bands that correspond to the even gaps. An increase in power to $\sim$18 dBm causes what appears to be a further splitting of the passband into equally wide regions of strong and weak transmission. We believe that this apparent splitting at 18 dBm is an artifact of the interference between the spin-wave signal and the low-level electromagnetic feedthrough. Beyond the auto-oscillation threshold, the output of the diode detector began to oscillate with a frequency of 10^4–10^6 Hz. Regions of strong auto-oscillations were located by measuring the peak-to-peak voltage $V_{\text{p.p.}}$ of the output signal. While density plots of S_{12} were obtained by sweeping the input frequency at a fixed input power, $V_{\text{p.p.}}$ was measured by sampling the output signal for 50 μs while the input parameters were kept constant. For the purpose of these measurements, the criterion used to establish the existence of auto-oscillations was when $V_{\text{p.p.}}$ exceeded 4 mV. At the bottom of Fig. 5 is a density plot of $V_{\text{p.p.}}$ over the selected region of our input parameter space. As is clearly evident, there appears to be a close correspondence between regions of low S_{12} and regions of high $V_{\text{p.p.}}$. At an input power of about 19 dBm, we note strong auto-oscillations at all frequencies. A careful examination reveals that the auto-oscillation threshold in the

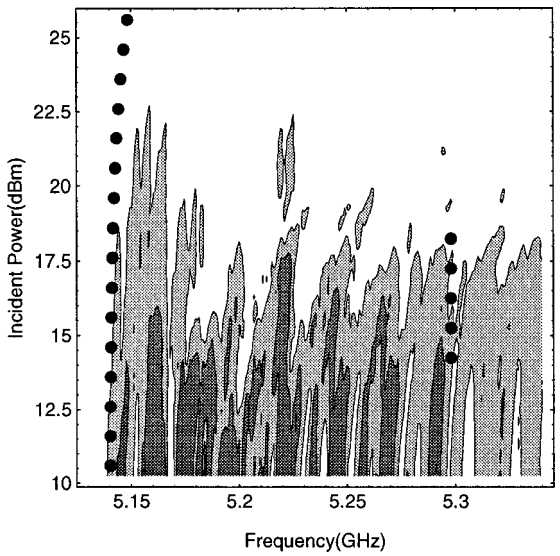

FIG. 7. Three-level contour plot of S_{12} using sample YIG2. The curved dark spots are the calculated locations for the edge of the passband. The vertical dark spots at 5.3 GHz are the locations where samples of the output microwave frequency spectrum were obtained. These spectra are shown in Fig. 8 and qualitatively demonstrate the correlation between a fingerlike region of weak transmission and the onset of auto-oscillations.

vicinity of a dipole gap is 4–8 dB lower than that outside the gap. A quantitative comparison between experimental results and theoretical predictions for a lower threshold inside a gap is undertaken in Sec. III C.

Experiments were also conducted on the two rectangular samples listed in Table I. Multipath interference resulting from reflections off the edge of these samples made it difficult to uniquely identify the dipole gaps in the passband. The density plots did successfully capture the saturation in S_{12} and the formation of fingers of low transmission. Figure 6 is a density plot of S_{12}, taken on sample YIG2, using 1-cm-long bidirectional transducers spaced 3 mm apart. Figure 7 is a three-level contour plot of the same data. A coarse contour plot emphasizes some global features while reducing the local variations that complicate the interpretation of a ten-level density plot. Figure 7 highlights the formation of fingerlike regions around 15 dBm (white regions extending down from above). The bottom of the passband shifted by approximately 10 MHz as the input microwave power was increased by 15 dB. This shift is reminiscent of previously established results on a shift in the passband at high-power levels.[24–26] A reduction in the demagnetizing field inside the film due to an increase in the cone angle of the precessing magnetization causes a shift that is given by[25]

$$\Delta\omega = \frac{-4\gamma P}{\omega M_s d^2}. \tag{10}$$

The shift is emphasized by the dotted curve on the left, which was calculated using Eq. (10) after alignment with the passband edge at low-power levels. Such effects were also observed on the $[BiLu]_3Fe_5O_{12}$ sample.[26] Note how Figs. 4 and 5 reveal a similar shift in the density plots of S_{12} and

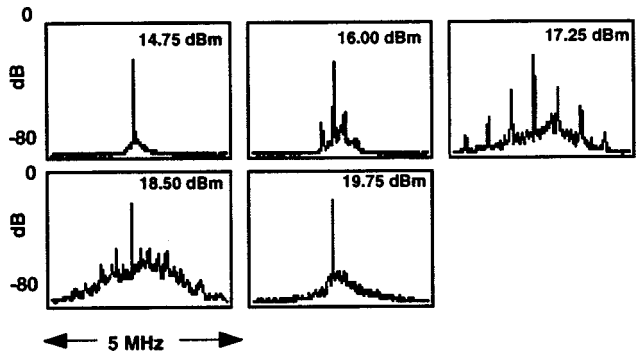

FIG. 8. Microwave frequency spectrum measured on a HP8529D spectrum analyzer. The input frequency was 5.3 GHz, while the input power was stepped between 14.75 and 19.25 dBm.

$V_{\text{p.p.}}$, thus establishing that the auto-oscillation thresholds are subject to the same demagnetizing effects as the transmission characteristics.

Auto-oscillations appeared in the output frequency spectrum as secondary peaks around the primary resonance frequency. As before, the fingerlike regions of low transmission were closely associated with regions in input parameter space where the output signal oscillated. For example, the dark spots in Fig. 7 at 5.3 GHz are the locations in parameter space where the output frequency spectrum was monitored. As shown in Fig. 8, the onset of auto-oscillations occurs as a finger of low transmitted power is crossed. The broad white regions reveal very complex routes to chaos, while their edges approximately mark the thresholds for the auto-oscillations.

III. THEORETICAL DISCUSSION

The density and contour plots of S_{12} capture not only a shift in the passband, a low-order nonlinear effect, but also help us locate the onset of auto-oscillations, a phenomenon that has its origins in a nonlinear four-magnon interaction.[3] A shift in the passband lends itself to a quantitative comparison with a theory based on an increasing precession angle for the magnetization.[27] However, the formation of fingers of auto-oscillation makes a comparison between theory and experimental observations for the auto-oscillation thresholds difficult. We explore the possibility that a finger of auto-oscillation is formed by a lower auto-oscillation threshold for spin waves with a lower group velocity. This phenomenon is easy to characterize in the vicinity of a dipole gap.

A. Transmission line model

A transmission line model for a MSW delay line sheds some light on the energy transferred into spin-wave modes in the vicinity of a dipole gap. Neglecting reactive impedance components, the fraction of power coupled into spin-wave modes is written as[20]

$$\frac{P_{\text{SW}}}{P_{\text{in}}} = \frac{4R_r R_g}{(R_r + R_g)^2}, \tag{11}$$

where P_{in} is the power fed into the device, $R_g = 50\ \Omega$ is the characteristic impedance of the transmission line, and R_r is the radiation resistance of the excited spin waves. R_r is esti-

mated for the case of spin waves pinned on both surfaces of the film using the method espoused by Dmitriev and Kalinikos.[28] Their calculations indicate that the radiation resistance in the vicinity of a dipole gap changes by a factor of order unity. We reevaluate their expressions for our device geometry and focus on the power coupled into spin-wave modes within an even-numbered dipole gap. For a ferromagnetic film, the linear radiative resistance is given by

$$R(\omega)=\frac{\mu_0\omega_M}{4}\sum_n \frac{\Omega_n Y_n^2}{v_{gn}}|j_k(k_{tn})|^2, \tag{12}$$

with a summation over all excited modes and k_{tn} representing the tangential wave number associated with the nth mode at frequency ω. Assuming $k_{tn}d\ll 1$ and a negligible separation between transducer and film,

$$k_{n-1}^2=k_{zn}^2+k_{tn}^2=\left(\frac{n\pi}{d}\right)^2+k_{tn}^2, \tag{13}$$

$$\Omega_n=\omega_H+\omega_M\lambda_{\mathrm{ex}}k_n^2, \tag{14}$$

$$Y_n\approx\frac{1}{\sqrt{d}}\frac{k_{zn}}{k_{tn}^2+k_{zn}^2}. \tag{15}$$

v_{gn} is the group velocity of the nth mode and $j_k(k_{tn})$ describes the surface current distribution in the microstrip transducer. $j_k(k_{tn})$ can be approximated by the zeroth-order Bessel function $J_0(k_{tn}w/2)$, where w is the width of the film. In this approximation, the dominant contributions to the sum in Eq. (12) come from modes that have lower values of k_{tn}. Consider exciting modes at the center of the nth dipole gap such that $\omega\approx\Omega_n$ and $k_{tn}=k_{t0}$. Thickness modes with mode numbers $m<n$ will have wave numbers $k_{tm}\gg k_{tn}$ and will thus be weakly excited, while higher-order modes with $m>n$ will not be excited. Consequently, the radiation resistance for the nth mode interacting with the lowest-order mode ($n=0$) becomes a sum of just two terms. Defining the resistance of the lowest-order mode as R_0, the resistance in the vicinity of the nth dipole gap is given by

$$R\approx R_0\left[1+\frac{\Omega_n}{\Omega_0}\left(\frac{Y_n}{Y_0}\right)^2\frac{v_{g0}}{v_{gn}}\right]=R_0(1+\epsilon_n). \tag{16}$$

Under the approximations $k_{tn}\ll k_{zn}$ and $\Omega_n\approx\Omega_H$,

$$\epsilon_n=\frac{1}{n^2}\left(\frac{v_{g0}}{v_{gn}}\right). \tag{17}$$

For the case of a transducer that is well matched to the lowest-order mode, $R_g=R_0$. Neglecting the small change in k_t as we move just outside the gap, the ratio of the power coupled into spin-wave modes inside a gap (P'_{SW}) to that coupled just outside the gap (P_{SW}) is calculated as

$$\frac{P'_{\mathrm{SW}}}{P_{\mathrm{SW}}}=\left(\frac{P'_{\mathrm{in}}}{P_{\mathrm{in}}}\right)\frac{4(1+\epsilon_n)}{(2+\epsilon_n)^2}. \tag{18}$$

The ratio of the group velocities is estimated using the equation[20]

$$\frac{1}{v_{gn}}=\frac{4\omega}{\omega_H\omega_M d}\left[1-\frac{n\pi\chi}{8}\right], \tag{19}$$

where χ is defined as

$$\chi=\frac{\omega_M\omega_H}{\omega_H^2-\omega^2}. \tag{20}$$

As the pumping frequency $\omega\rightarrow\omega_n$, Eqs. (3), (17), (19), and (20) are combined to yield

$$\epsilon_n\approx\frac{-\pi\chi}{8n}=\frac{d^2}{16\lambda_{\mathrm{ex}}\pi n^3}. \tag{21}$$

Based on the previously described experiments on sample YIG1, for $n=20$, $\epsilon_n\approx 0.4$ and the fraction of power coupled into the spin-wave system is largely constant over the entire passband. In our experiments, moving into the dipole gap caused a decrease in the power coupled into the device of less than 10%, qualitatively supporting the above theoretical calculation.

B. Auto-oscillation thresholds

Consider the spin-wave instability of forward-volume waves when the pumping field is perpendicular to the static external magnetic field, often called the second Suhl instability. Suhl recognized that the spin-wave amplitude at the main resonance begins to increase exponentially once the amplitude of the uniform mode, $|a_0|$, satisfies the condition[29]

$$\xi_k^2|a_0|^4>(\omega-\omega_k)^2+\eta_k^2, \tag{22}$$

η_k being the damping constant. For small values of k, $\xi_k\sim\omega_M$ and $\omega_k\rightarrow\omega_H$. As before, ω_H defines the edge of the passband. Suhl predicted a saturation of the main resonance beyond the critical value, with the excess energy being coupled into other spin waves via a nonlinear mechanism.[29] The damping constants $\eta_0(\omega_H)$ and $\eta_k(\omega_k)$ are related to the FMR linewidth (ΔH measured at a frequency ω') as[30]

$$\eta_0=\frac{|\gamma|\mu_0\omega_H}{2}\left(\frac{\Delta H}{\omega'}\right), \tag{23}$$

$$\eta_k=\frac{\eta_0}{\omega_H}\left[\frac{\omega_H^2+\omega_k^2}{2\omega_k}\right]. \tag{24}$$

The linear solution for a_0 in the presence of a pumping field h is

$$a_0=\frac{|\gamma|\mu_0 h}{(\omega_H-\omega)+i\eta_0}. \tag{25}$$

For a pumping frequency $\omega=\omega_H$, the critical value of the pumping field at the second Suhl instability (SI) is estimated to be

$$h_{\mathrm{SI}}\approx\frac{\eta_0}{|\gamma|\mu_0}\sqrt{\frac{\eta_k}{\omega_M}}. \tag{26}$$

These are the results associated with a stationary solution to the nonlinear Hamiltonian equations of motion.[3] The nonstationary process leading to auto-oscillations has a threshold field value of[7]

$$h_{\mathrm{AO}} \approx 4 h_{\mathrm{SL}}. \tag{27}$$

To calculate the magnetic field associated with the lowest-order MSW's, we return to the description of the magnetostatic potential given in Eq. (4). The magnetic field is defined as $-\nabla\psi$, and as $\omega \rightarrow \omega_H$, its amplitude at the center of the film is given by

$$\lim_{z\rightarrow 0}|h| = |-\nabla\psi| = |k_t \psi_0| \approx \left|\frac{-2}{\chi d}\psi_0\right|. \tag{28}$$

Using Eqs. (5) and (28), the input power required to reach the critical field h_{AO} for our thin film geometry is found to be

$$P_{\mathrm{AO}}[\mathrm{mW/mm}] = \frac{1}{8}\omega\mu_0 h_{\mathrm{AO}}^2 d^2 |\chi|^2. \tag{29}$$

At the edge of the passband, $k_t \rightarrow 0$ and $|\chi| \rightarrow \infty$, resulting in a divergence of the critical power. The singularity at the edge of the passband is a consequence of our earlier definition for χ, in Eq. (20), where we neglected the lossy characteristics of the film. Introducing a loss parameter,

$$\chi = \frac{(\omega_H - i\eta_k)\omega_M}{(\omega_H - i\eta_k)^2 - \omega_k^2}. \tag{30}$$

This form for χ is analytic at the lower edge of the passband. Typically, $n_0 \ll \omega_H$, and as $\omega_k \rightarrow \omega_H$,

$$|\chi| \approx \frac{\omega_M}{2\eta_0}. \tag{31}$$

Combining Eqs. (26), (27), (29), and (31), the expression for the critical power in the limit $k \rightarrow 0$ is written as

$$P_{\mathrm{AO}} = \frac{\omega_H \omega_M \eta_0 d^2}{2|\gamma|^2 \mu_0}. \tag{32}$$

Assuming well-matched transducers, i.e., $R_g \approx R_r = R_0$ in Eq. (11), $P_{\mathrm{in}} \approx P_{\mathrm{AO}}$ defines the threshold input power required to observe auto-oscillations.

Words of caution are necessary at this juncture. In the spirit of the calculation, the effects of a ground plane on the excitation of MSW's have been neglected. Outside the film, the magnetostatic potential $\psi \sim e^{-k_t z}$. For a spacing s between the film and ground plane, the effects of the ground plane become important when $(ks) < 1$. Neglecting the effects of the ground plane is merely a good starting approximation.

Density plots of S_{12} were also obtained for the other two samples.[8,26] Using Eq. (32), the input power required to observe auto-oscillations is estimated for each of the samples. The calculation accounts for the fact that the device consists of a bidirectional transducer, but assumes that the reflected power from the device is negligible. The calculated critical power for the three films used, in the $\omega_k \rightarrow \omega_H$ limit, is given in Table II. The experimental value is determined as the approximate power level at which a saturation in S_{12} was observed in a density plot.

TABLE II. Experimental and theoretical values for the critical power corresponding to the threshold for auto-oscillations. The theoretical value was calculated using Eq. (32), while the experimental values were obtained by studying density plots of S_{12}.

Film	$\omega_H/(2\pi)$ (GHz)	$\eta_0(\times 10^6)$ (rad/s)	P_{theory} (dBm)	P_{expt} (dBm)
YIG1	4.4	2.5	12.8	13-19
YIG2	5.1	4.3	17.7	14-18
BLIG	7.3	21.2	24.9	24-28

C. Formation of fingers

A finger of auto-oscillation is merely a small set of pumping frequencies at which auto-oscillations occur at a lower threshold than at neighboring frequencies. Without a complete characterization of all the interacting spin waves, a quantitative calculation of the thresholds is quite *ad hoc*. However, the following dimensional analysis reveals that the auto-oscillation threshold will be lower at frequencies within a dipole gap. The average power per unit width P can be expressed in terms of the average energy density $\langle E\rangle$, the thickness of the film, and the group velocity as

$$P = \langle E\rangle v_g d, \tag{33}$$

where $\langle E\rangle \propto |h|^2$. Consider the frequencies ω' and ω such that $|\omega - \omega'| \ll \omega$ and $\eta_k \approx \eta_{k'}$, with the primed variables representing quantities within a dipole gap and the unprimed ones just outside the gap. With the understanding that $\langle E\rangle$ must thus have the same value at the auto-oscillation threshold both inside and outside a gap, Eqs. (18) and (33) are combined and rewritten as

$$\frac{P_{\mathrm{in}}}{P'_{\mathrm{in}}} = \frac{v_g}{v'_g}\frac{4(1+\epsilon_n)}{(2+\epsilon_n)^2}, \tag{34}$$

where n is the mode number associated with the dipole gap under consideration and ϵ_n is related to the ratio of the asymptotic values of the group velocity as defined in Eq. (17). However, the ratio $v_g/v'_g \neq n^2\epsilon_n$ and must be determined after accounting for a change in the dispersion relation in the vicinity of a dipole gap.

Following the analysis by Kalinikos and Slavin, the splitting of the MSW dispersion relation is quantified using a perturbation series.[18] (Note that owing to a different numbering scheme, symmetric modes with totally pinned surface spins have even numbers in our calculations, but have odd numbers in the theory of Kalinikos and Slavin.) The secular equation that describes an interaction between even modes takes the form

$$(\omega_n^2 - \omega_{nn'}^2)(\omega_{n'}^2 - \omega_{nn'}^2) = \omega_M^2 \Omega_n \Omega_{n'} F_{nn'}^2, \tag{35}$$

where

$$\omega_n^2 = \Omega_n(\Omega_n + \omega_M F_{nn}), \tag{36}$$

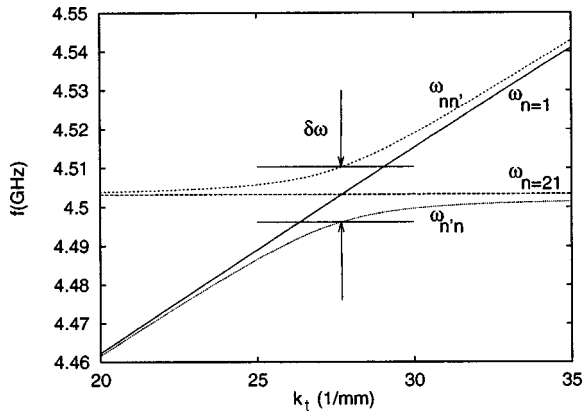

FIG. 9. MSW dispersion relation showing the interaction between the $n=0$ and $n'=20$ thickness modes as a function of tangential wave number k_t, calculated using $n=1$ and $n'=21$ in Eqs. (35) and (36).

$$F_{nn'}=\frac{k_t^2}{k_{n'}^2}\delta_{nn'}+\frac{k_t^2 k_{zn}k_{zn'}}{k_n^2 k_{n'}^2}\left[\frac{2}{k_t d}(1+e^{-k_t d})\right]. \tag{37}$$

k_{zn} and Ω_n are as defined in Eqs. (13) and (14), respectively, and $\delta_{nn'}$ is a Kronecker delta function. Note that Eq. (36) reduces to Eq. (3) when $\omega_M F_{nn} \ll \Omega_n$. The dispersion relation for the case $n=0$, $n'=20$ is shown in Fig. 9. The width of the dipole gap $\delta\omega$ is determined by the splitting between the two branches of the dispersion relation $\omega_{nn'}$ and $\omega_{n'n}$ as shown in the figure.

The group velocity of a spin wave decreases in the vicinity of a dipole gap. v_g is calculated numerically from the curves in Fig. 9 and is shown in Fig. 10. The width of the gap is marked by a pair of arrows, corresponding to similar arrows in Fig. 9. Although it appears that the group velocity decreases to its asymptotic value as given by the slope of $\omega_{n=20}$, the effects of such a low value are not observed in our experiments. As v_g decreases, the propagation loss for the spin waves between transducers increases. Assuming that the amplitude of the auto-oscillations decays at the same rate as that of the spin waves, a threshold value for $V_{\text{p.p.}}$ sets a minimum detectable value for v_g. Let the decay in the amplitude of auto-oscillations between transducers spaced a distance L apart be described by

$$\phi \propto e^{-\eta_k L/v_g}. \tag{38}$$

In the experiment described in Sec. II B, with a transducer spacing of 4 mm, $V_{\text{p.p.}}$ varied from the threshold value of 4 mV to a maximum of 20 mV. As was seen in Fig. 5, the lowest auto-oscillation thresholds were observed inside the gap. Attributing the different auto-oscillation amplitudes to attenuation resulting from variation in group velocity, a comparison of the decay in auto-oscillations at locations inside and outside a gap yields

$$\frac{V'_{\text{p.p.}}}{V_{\text{p.p.}}}=\frac{\phi'}{\phi}=\exp\left[-\eta_k L\left(\frac{1}{v'_g}-\frac{1}{v_g}\right)\right]\approx\frac{1}{5}. \tag{39}$$

For the sample YIG1, $\eta_k \approx \eta_0 = 2.4\ \mu\text{s}^{-1}$ and, as seen from Fig. 10, $v_g \approx 32$ km/s. Hence,

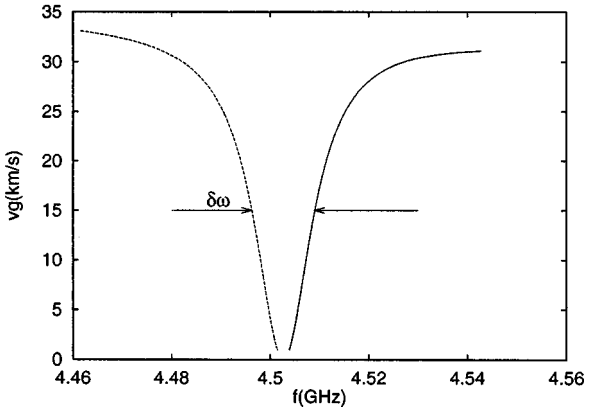

FIG. 10. Group velocity in the vicinity of a dipole gap. The data were obtained by numerically differentiating $\omega_{nn'}$ and $\omega_{n'n}$ in Fig. 9.

$$\left(\frac{v_g}{v'_g}\right)_{\max}\approx 6.1. \tag{40}$$

A minimum value for v_g/v'_g can be determined directly from Fig. 10. At a frequency at the edge of the gap, marked by an arrow, v_g is smaller by a factor of about 2.2 compared to its maximum value. The range of values, $2.2 < v_g/v'_g < 6.1$, determines the approximate range for the auto-oscillation threshold. When translated into power levels using Eq. (34), the auto-oscillation threshold observed within a dipole gap should be 3–8 dB lower than the threshold value outside the gap. As seen in Fig. 5, this range of values compares favorably with the experimentally observed decrease in thresholds associated with the fingers. A lower threshold combined with the shift in the passband causes the formation of a finger of auto-oscillation.

IV. CONCLUSIONS

Large-amplitude spin waves often undergo nonlinear interactions. As a result of these interactions, the output from a forward-volume MSW delay line develops an amplitude modulation with multiple frequency components. This phenomenon is commonly referred to as auto-oscillation and is accompanied by a drop in the dc value of the output signal. The S_{12} transmission characteristics of a delay line were studied using three different samples over a two-dimensional input parameter space comprising of input power and frequency. Density and contour plots were useful tools in this venture. A shift in the MSW passband at high input powers was easily captured by the plots. This shift has been attributed to a decrease in the demagnetizing field as the dynamic magnetization was increased. The shift was of the same order as that predicted by other researchers.[24,25] Furthermore, a comparison of a density plot of S_{12} with a similar plot for the amplitude of auto-oscillations revealed a close correlation between the formation of fingers of low transmission and the formation of fingers of auto-oscillation.

The threshold power levels required to observe auto-oscillations in thin films, when extrapolated to the $k \to 0$ limit, seemed to agree with the theoretical predictions for

auto-oscillations in an infinite medium.[7] Previous models have explained the formation of fingers of auto-oscillation for the case of standing-wave modes.[13] In the case of pinned-surface spin waves propagating between two transducers, the simultaneous excitation of two thickness modes causes a reduction in the group velocity of the waves and the formation of a dipole gap. Consequently, there is a decrease in the power levels required to maintain a critical energy density inside the film. A heuristic model that used this argument described the formation of a finger of auto-oscillation. The predicted decrease in auto-oscillation threshold power levels in the vicinity of a dipole gap was comparable to that observed experimentally.

ACKNOWLEDGMENTS

We are grateful to A. Slavin for some very illuminating discussions on the theoretical aspects of nonlinear spin-wave interactions. By sharing with us their experimental results on spin-wave solitons, P. Kabos and C. E. Patton have given us much assistance. We also thank J. D. Adam and J. Peruyero for providing us with the samples used. This work was supported in part by the National Science Foundation under Grant No. ECS-9206817.

*Current address: MKE-Quantum, 1450 Infinite Dr., Louisville, CO 80027.

[1] *Linear and Nonlinear Spin Waves in Magnetic Films and Superlattices*, edited by M. Cottam (World Scientific, Singapore, 1994).

[2] *Nonlinear Phenomena and Chaos in Magnetic Materials*, edited by P. Wigen (World Scientific, Singapore, 1994).

[3] V. S. L'vov, *Turbulence under Parametric Excitation, Applications to Magnets* (Springer-Verlag, Berlin, 1994).

[4] *High Frequency Processes in Magnetic Materials*, edited by G. Srinivasan and A. Slavin (World Scientific, Singapore, 1995).

[5] G. Gibson and C. Jeffries, Phys. Rev. A **29**, 811 (1984).

[6] P. H. Bryant, C. D. Jeffries, and K. Nakamura, Phys. Rev. A **38**, 4223 (1988).

[7] X. Y. Zhang and H. Suhl, Phys. Rev. B **38**, 4893 (1988).

[8] A. Prabhakar and D. D. Stancil, J. Appl. Phys. **79**, 5374 (1996).

[9] T. L. Carroll, L. M. Pecora, and F. J. Rachford, Phys. Rev. Lett. **59**, 2891 (1987).

[10] F. M. Aguiar, A. Azevedo, and S. M. Rezende, J. Appl. Phys. **73**, 6825 (1993).

[11] M. Ye, D. E. Jones, and P. E. Wigen, J. Appl. Phys. **73**, 6822 (1993).

[12] M. Ye, D. W. Peterman, and P. E. Wigen, Phys. Lett. A **203**, 23 (1995).

[13] R. D. McMichael and P. E. Wigen, Phys. Rev. B **42**, 6723 (1990).

[14] R. D. McMichael and P. E. Wigen, Phys. Rev. Lett. **64**, 64 (1990).

[15] R. E. deWames and T. Wolfram, J. Appl. Phys. **41**, 987 (1970).

[16] T. Wolfram and R. E. DeWames, Phys. Rev. B **4**, 3125 (1971).

[17] J. D. Adam, T. W. O'Keefe, and R. W. Patterson, J. Appl. Phys. **50**, 2446 (1979).

[18] B. Kalinikos and A. N. Slavin, J. Phys. C **19**, 7013 (1986).

[19] D. D. Stancil and A. Prabhakar, in *Nonlinear Microwave Signal Processing: Towards a new range of devices*, edited by R. Marcelli and S. A. Nikitov (Kluwer Academic, Dordrecht, 1996), Chap. 17, p. 467.

[20] D. D. Stancil, *Theory of Magnetostatic Waves* (Springer-Verlag, New York, 1993).

[21] E. H. Turner, Phys. Rev. Lett. **5**, 1295 (1958).

[22] P. A. Kolodin, E. G. Rzhikhina, and A. N. Slavin, Sov. Phys. Tech. Phys. **35**, 951 (1991).

[23] A. K. Chernakova, A. Cash, J. Peruyero, and D. D. Stancil, J. Appl. Phys. **75**, 6066 (1994).

[24] M. A. Tsankov, M. Chen, and C. E. Patton, J. Appl. Phys. **79**, 1595 (1996).

[25] A. Cash and D. D. Stancil, IEEE Trans. Magn. **32**, 5188 (1996).

[26] A. Prabhakar and D. D. Stancil, IEEE Trans. Magn. **32**, 4174 (1996).

[27] D. D. Stancil and N. Bilaniuk, in *High Frequency Processes in Magnetic Materials*, edited by G. Srinivasan and A. Slavin (World Scientific, Singapore, 1995), Chap. 10, pp. 357–393.

[28] V. F. Dmitriev and B. Kalinikos, Izv. Vyssh. Uchebn. Zaved. Fiz. **31**, 875 (1988) [Sov. Phys. J. **31**, 875 (1988)].

[29] H. Suhl, J. Phys. Chem. Solids **1**, 209 (1957).

[30] D. D. Stancil, J. Appl. Phys. **59**, 218 (1986).